Direct numerical simulation of transitional pulsatile stenotic flow using Lattice Boltzmann Method

In the present work, I perform direct numerical simulations of pulsatile flow through a 75% eccentric stenosis using the Lattice Boltzmann Method. The stenosis was studied by Varghese et al. (2007b) in a benchmark computation and the goal of this work is to validate the LBM solver Musubi for transitional flows in anatomically realistic geometries. Whereas most of the study reproduces and compares simulation results from Musubi against the benchmark, the latter part quantifies the Kolmogorov micro-scales and discusses the role of space and time resolutions for the simulation of a transitional flow. The LBM results show an excellent agreement with the previously published results thereby increasing confidence on our Musubi solver for the simulation of transitional flows. The aim of this study is not to compare the computational efficiency of the code or the method but only the physics of the flow.

PeerJ PrePrints | https://doi.org/10.7287/peerj.preprints.1548v1 | CC-BY 4.0 Open Access | rec: 30 Nov 2015, publ: 30 Nov 2015

Direct numerical simulation of transitional pulsatile stenotic flow using Lattice Boltzmann Method

Kartik Jain *[1,2]

[1] *Simulation Techniques and Scientific Computing, University of Siegen, Hölderlinstr. 3, 57076 Siegen, GERMANY*
[2] *Center for Biomedical Computing, Simula Research Laboratory, N-1325 Lysaker, NORWAY*

Abstract

In the present work, I perform direct numerical simulations of pulsatile flow through a 75% eccentric stenosis using the Lattice Boltzmann Method. The stenosis was studied by Varghese *et al.*[28] in a benchmark computation and the goal of this work is to validate the LBM solver *Musubi* for transitional flows in anatomically realistic geometries. Whereas most of the study reproduces and compares simulation results from *Musubi* against the benchmark, the latter part quantifies the Kolmogorov micro-scales and discusses the role of space and time resolutions for the simulation of a transitional flow.

The LBM results show an excellent agreement with the previously published results thereby increasing confidence on our *Musubi* solver for the simulation of transitional flows. The aim of this study is not to compare the computational efficiency of the code or the method but only the physics of the flow.

1 Introduction

Direct numerical simulation is a way of numerically simulating flow in arbitrary geometries by resolving all the temporal and spatial scales that might appear in a transitional or a turbulent flow. Consequently this technique requires very high spatial and temporal resolutions and more compute power. Spectral methods and classical computational fluid dynamic (CFD) techniques like finite element method (FEM) and finite volume method (FVM) have been commonly employed for the simulation of flows. Spectral methods indeed are the most well established technique for the simulation of transitional flows as they allow for an increase in effective resolution easily. In complex anatomical geometries

*Corresponding Author; E-mail: kartik.jain@uni-siegen.de; Phone: +49-271-740-3882

PeerJ PrePrints | https://doi.org/10.7287/peerj.preprints.1548v1 | CC-BY 4.0 Open Access | rec: 30 Nov 2015, publ: 30 Nov 2015

however, which are the main goal of my work still are difficult to be computed using spectral methods.

The Lattice Boltzmann Method (LBM) is an alternative technique for the simulation of low Mach number incompressible flows[24;12;15;16]. Although well established, due to its novelty the LBM has met with criticism and skepticism, much of which is attributed to its *indirect* nature i.e. the method converges to the incompressible Navier-Stokes equations under the continuum limits of low Mach and Knudsen numbers[12;21]. A comparison of LBM with spectral methods by Succi *et al.*[24] suggested excellent agreement although much work was not done in this direction after that.

Our LBM solver *Musubi*[7;6;14] was specifically designed for high performance computing architectures to address large scale problems, and it scales on all the federal compute resources of Germany namely *Juqueen*, *SuperMUC* and the *Hazel Hen*. *Musubi* solver, even though is verified and validated thoroughly[7;6] for laminar and turbulent flows, a thorough validation has not been done for transitional and pulsating flows[1]. Swayed by the need for validation, and in support of its extensive use in my simulations of transitional physiological flows, this work re-simulates the pulsatile flow through the eccentric stenosis that was previously studied in[27;28].

Since the emphasis is on the LBM, I will particularly focus on the role of parameters like the relaxation scheme of LBM, and space and time resolutions in *reproducing* results of previous DNS reported in[28]. To assess the quality of DNS, I will compute and quantify the Kolmogorov length and time scales, and will discuss the conditions under which going down to these scales might benefit the engineer while simulating physiological flows.

The results show an excellent agreement with Varghese *et al.*[28] thereby increasing the confidence on the LBM and the solver *Musubi* for such applications. The Kolmogorov micro-scales and the recommendations that are provided in this chapter can be referenced for in future for purposes of comparison.

2 Methods

The eccentric stenosis geometry used for this study was similar to the models employed in the experiments of stenotic flow by[1;2]. The stenosis axis was offset by 0.05D, D being the vessel diameter, in the eccentric model. The eccentric stenosis geometry used for simulations is shown in figure 1(a). The offset of 0.05D from the axisymmetric counterpart (not studied here) is represented in figure 1(b), where the dashed line shows the eccentric case and black shows the axisymmetric. The pre and post-stenotic regions of the vessel were respectively extended by 3 and 18 vessel diameters as measured from the throat of stenosis.

The Womersley solution for laminar, pulsatile flow through rigid tubes was used as

[1] *Musubi*, along with its colleagues within our APES framework is available as an open source tool for download under: https://bitbucket.org/apesteam/musubi

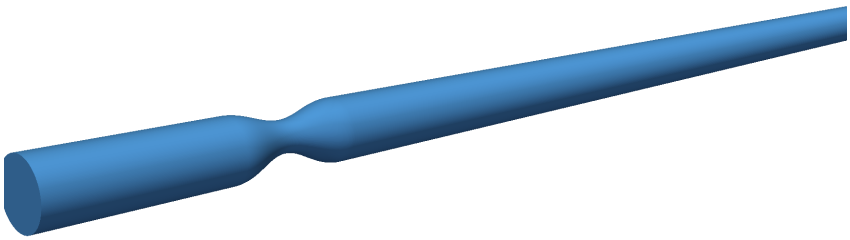

(a) stenosis geometry

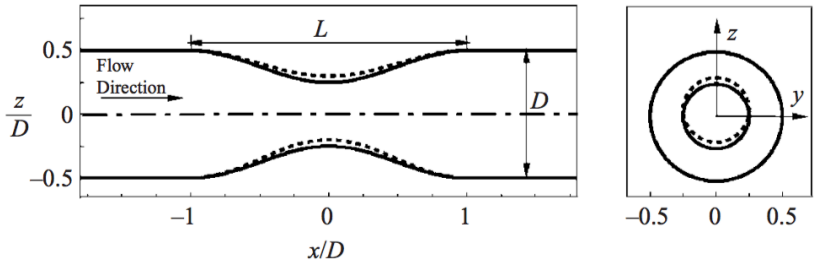

(b) offset from the symmetric stenosis that introduces eccentricity

Figure 1: The eccentric geometry of stenosis used in the study. Lower part of the figure shows front and side views of the stenosis where solid line denotes the axisymmetric model and dashed line denotes the eccentric case. x is the streamwise direction and y and z are cross-stream directions.

inlet boundary condition, which is specified as:

$$\left.\begin{aligned} \frac{u_x}{u_c} &= [1-r^2] + A\left[1 - \frac{J_0(i^{3/2}\alpha 2r/D)}{J_0(i^{3/2}\alpha)}\right] sin(\omega t), \\ \frac{u_y}{u_c} &= 0, \\ \frac{u_y}{u_c} &= 0 \end{aligned}\right\} \quad (1)$$

where u_c is the cycle-averaged centerline inlet velocity, A is the amplitude of pulsation, J_0 is the Bessel function of type 0, ω is the angular frequency of pulsation, and α is the non-dimensional Womersley parameter ($= \frac{1}{2}D\sqrt{\omega/\nu}$, where ν is the kinematic viscosity). The Womersley parameter defines the extent to which the laminar profile departs from quasi-steadiness, an effect that becomes significant when $\alpha = 3$.

The parameters and normalizations mentioned above are chosen to replicate the flow conditions of experiments of Ahmed & Giddens[2] and simulations of Varghese *et al.*[28]. The Reynolds number based on the main vessel diameter, D, and the mean inlet centerline velocity, u_c was 600 with minima and maxima of 200 and 1000. The value of A was 0.667 in equation 1. The Womersley number α was 7.5. The velocity waveform at the inlet was sinusoidal and recordings were made in intervals of T/6 where T is the period of pulsation (depicted in figure 2).

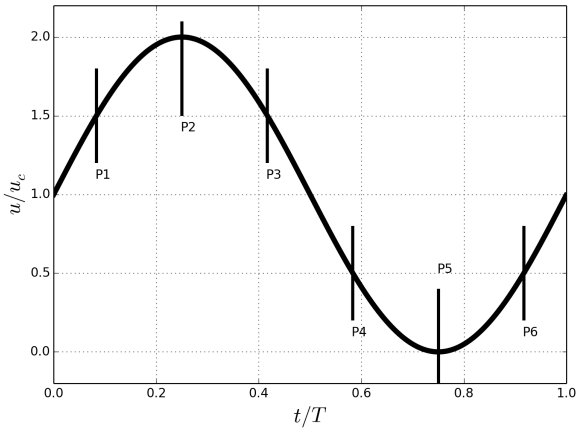

Figure 2: Axial centerline velocity at the vessel inlet. The measurements were made at 6 time points in the sinusoidal cycle that are indicated in the plot.

	δx	δt	#Cells diameter	#Cells throat	#Cells
LR	64	30×10^{-6}	156	40	$\sim 83 \times 10^6$
HR	32	7.5×10^{-6}	312	80	$\sim 680 \times 10^6$

Table 1: The spatial and temporal discretization of eccentric stenosis. The space and time have been non-dimensionalized and of relevance here is the number of cells along the diameter and stenotic throat.

Direct Numerical Simulations

The simulation tool chain is contained in our end-to-end parallel framework APES (adaptable poly engineering simulator)[23;14]. Meshes were created using the mesh generator *Seeder*[5]. I have used the single relaxation scheme Bhatnagar-Gross-Krook (BGK) out of the various LBM relaxation schemes implemented in *Musubi*. I performed two sets of simulations – one with moderate/low resolutions (LR) and one with extremely high resolutions (HR), down to the Kolmogorov microscales. The resulting parameters are listed in table 1. The space and time have been non-dimensionalized for the simulation, and the things to note are the number of lattice cells along the diameter of the main channel and that along the throat of the stenosis. The time step is coupled with the grid spacing in LBM as $\delta t \sim \delta x^2$, which reflects the *diffusive time scaling* necessary to recover the incompressible Navier-Stokes equation from the Lattice Boltzmann Equation[12]. The BGK relaxation parameter was set to $\Omega = 1.94$ in the present study that keeps the lattice Mach number within the stability limits of the LBM[17;21]. The vessel walls were assumed to be rigid and a no-slip boundary condition, described by a bounce-back rule in LBM was prescribed[2]. The D3Q19 stencil of the LBM algorithm was employed which means 19 discrete velocity directions per fluid cell, or 19 degrees of freedom. Stencils with larger

[2]It should be mentioned that I have intentionally not used the higher order wall approximation of LBM boundaries because my goal was to try and simulate the flow with simplest LBM techniques possible

number of degrees of freedom can be employed but it has previously been suggested that the gain in accuracy for low Re flows is not appreciable compared to the cost of memory and computation[19]. At the outlets, zero pressure was prescribed which is described by a high-order extrapolation in the LBM algorithm[13].

LR and HR computations were executed using 1000 and 9600 cores respectively of the *Hazel Hen* supercomputer installed at the High Performance Computing center in Stuttgart, Germany. The *Hazel Hen* contains a total of 185 088 cores of Intel(R) Xeon(R) CPU E5-2680 v3 (30M Cache, 2.50 GHz). *Hazel Hen* is one of the main federal compute resources in Germany and is ranked at number 8 in the current listing of top supercomputers[3]. Computation of each cycle required $\sim$ 36 minutes for LR simulations and $\sim$ 32 minutes for the HR simulations[4]. A detailed account of the performance and scalability of *Musubi* can be found elsewhere[7;14].

Flow analysis

The analysis of a turbulent or transitional flow follows the statistical principles as statistics, due to the chaotic behavior of the flow are the only reproducible quantities[20;3]. A total of $n = 22$ (where initial 2 cycles are discarded from analysis) cycles were computed from both LR and HR simulations and were ensemble averaged for analysis. The ensemble average over **n** cycles is defined as:

$$\overline{u}(x,t) = \frac{1}{n}\sum_{k=0}^{n-1} u(x, t + kT) \tag{2}$$

where $u(x,t)$ is the instantaneous point wise velocity field, **x** denotes the spatial coordinates, **t** is the time and **T** is the period of cardiac cycle. The instantaneous three-dimensional velocity field was decomposed into a mean and a fluctuating part using Reynolds' decomposition i.e.

$$u_i(x,t) = \bar{u_i}(x) + u_i'(x,t) \tag{3}$$

The Turbulent Kinetic Energy (TKE) is derived from the fluctuating components of the velocity in 3 directions as:

$$k = \frac{1}{2}\left(u_x'^2 + u_y'^2 + u_z'^2\right) \tag{4}$$

A power spectral density of the TKE, computed using Fourier transforms provides information about the frequency components present in the flow, and can be related to the Kolmogorov energy decay.

[3]http://top500.org

[4]The computation time mentioned is not comparable with Varghese *et al.*[28] as those computations were done in 2007 using a completely different architecture and CPUs, and a comparison of computational efficiency is not the intention of this study

111 ## The Q-criterion

The Q-criterion was preferred in the present study for the visualization of coherent flow structures as it shares properties with both the vorticity and pressure criterion[9]. The Q-criterion is the second invariant of the velocity gradient tensor $\nabla \mathbf{u}$, and reads:

$$Q = \frac{1}{2}(\Omega_{ij}\Omega_{ij} - S_{ij}S_{ij}) \tag{5}$$

where

$$\Omega_{ij} = \frac{1}{2}\left(\frac{\partial u_i}{\partial x_j} - \frac{\partial u_j}{\partial x_i}\right) \tag{6}$$

and

$$S_{ij} = \frac{1}{2}\left(\frac{\partial u_i}{\partial x_j} + \frac{\partial u_j}{\partial x_i}\right) \tag{7}$$

112 are respectively the anti-symmetric and symmetric components of $\nabla \mathbf{u}$.

The Q-criterion can be physically viewed as the balance between the rotation rate $\Omega^2 = \Omega_{ij}\Omega_{ij}$ and the strain rate $S^2 = S_{ij}S_{ij}$. Positive Q isosurfaces confine the areas where the strength of rotation overcomes the strain - making those surfaces eligible as vortex envelopes. Several interpretations of Q-criterion have been proposed, see for example Robinson[22] which recasts Q in a form which relates to the vorticity modulus ω:

$$Q = \frac{1}{4}(\omega^2 - 2S_{ij}S_{ij}). \tag{8}$$

113 This implies that the Q is expected to remain positive in the core of the vortex as vorticity
114 increases as the center of the vortex is approached.

115 ## DNS quality assessment with Kolmogorov microscales

The smallest structures that can exist in a turbulent flow are based on Kolmogorov's theory[20]. Viscosity dominates and the TKE is dissipated into heat at the Kolmogorov scale[20]. The Kolmogorov microscales are generally described in terms of the rate of dissipation due to turbulent kinetic energy, which results in equations containing 4th order terms[20;3]. The Kolmogorov scales, for simplicity, can also be computed in terms of local friction velocity $u_* = \sqrt{\nu||s||}$ where s_{ij} is the *fluctuating* component of strain rate defined as:

$$s_{ij} = \frac{1}{2}\left(\frac{\partial u_i'}{\partial x_j} + \frac{\partial u_j'}{\partial x_i}\right) \tag{9}$$

116 and ν is the kinematic viscosity.

The Kolmogorov length, time and velocity scales are then respectively estimated as:

$$\eta \equiv \nu/u_* \tag{10}$$

$$\tau_\eta \equiv \nu/u_*^2 \tag{11}$$

$$u_\eta \equiv u_* \tag{12}$$

Based on these scales, the quality of the spatial and temporal resolution of a simulation is estimated by computing the ratio of δx and δt against corresponding Kolmogorov scales i.e.

$$l^+ = \frac{u_* \delta x}{\nu}. \tag{13}$$

$$t^+ = \frac{u_*^2 \delta t}{\nu}. \tag{14}$$

Ideally these ratios should be $\sim$ 1 but in practice it has been observed that a l^+ of the order of $\mathcal{O}(10)$ is usually enough for the simulation of moderate Reynolds' numbers transitional flows[18].

3 Results

Figure 3(a) and 3(b) depict the axial centerline velocities over the last $n = 6$ cycles obtained from LR and HR simulations respectively. Ensemble averaged counterparts for $n = 20$ cycles are shown in figure 4(a) and 4(b). Whereas the main flow captured by LR and HR simulations is similar, high resolutions capture higher fluctuations particularly in post-stenotic regions (x=3-5D) and the differences between LR and HR are mostly visible in time periods when the slow starts to decelerate. This observation would characterize LR setup as *converged*, though as would be seen in the turbulent characteristics, some intricate features might be suppressed by low resolutions.

The ensemble averaged quantities look largely similar for LR and HR simulations as the minute dynamics that were captured by HR are smeared out upon averaging. Subtle differences remain in the post-stenotic regions due to higher gradients in these regions. The remainder of the text would thus employ LR simulation results when ensemble averaged quantities are discussed and HR will be talked about only when instantaneous quantities are of interest.

Figure 5 and 6 respectively show the upstream velocity field in xz and xy axial bisecting planes. The velocity is ensemble averaged for n=20 cycles after 2 initial cycles that have been discarded from analysis. Corresponding plots from Varghese *et al.*[28] are also shown below each plot computed from *Musubi* for a direct visual comparison.

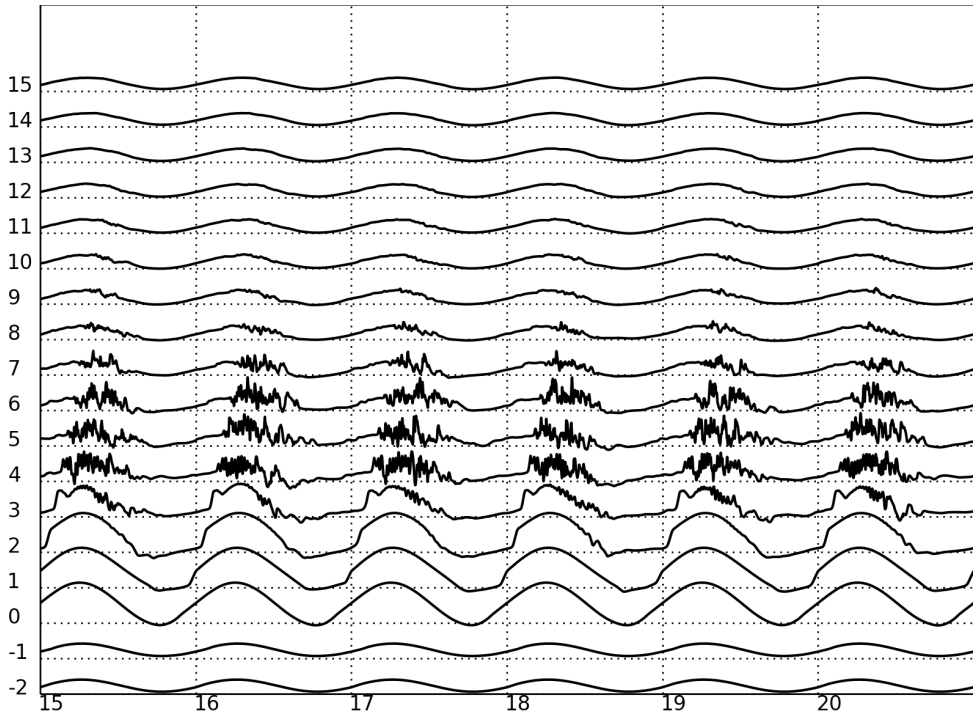

(a) LR

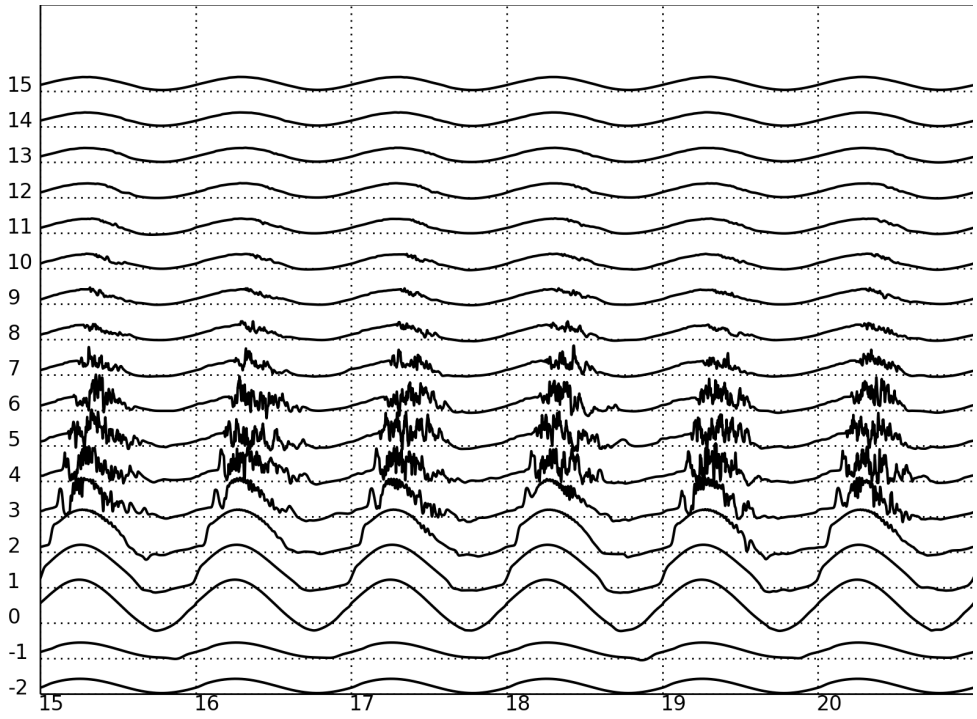

(b) HR

Figure 3: Temporal evolution of the normalized centerline axial velocity, u/u_c over the last 6 cycles out of total 20 that were simulated, as a function of axial distance through stenosis, shown for LR and HR simulations.

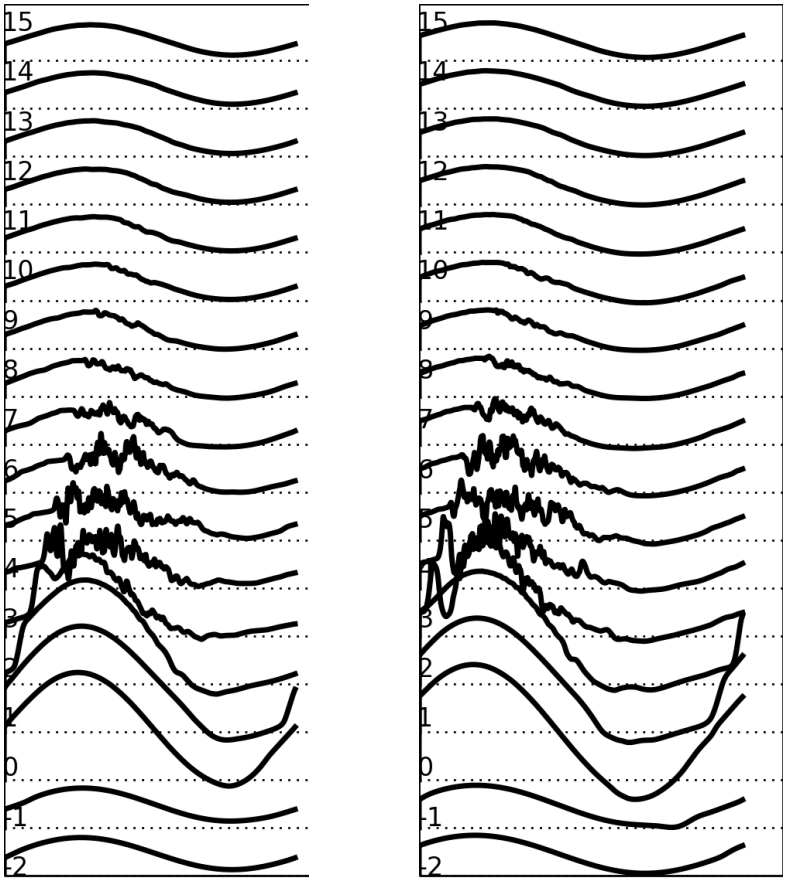

(a) LR (b) HR

Figure 4: Normalized centerline axial velocity ensemble averaged for $n = 20$ cycles shown for LR and HR simulations.

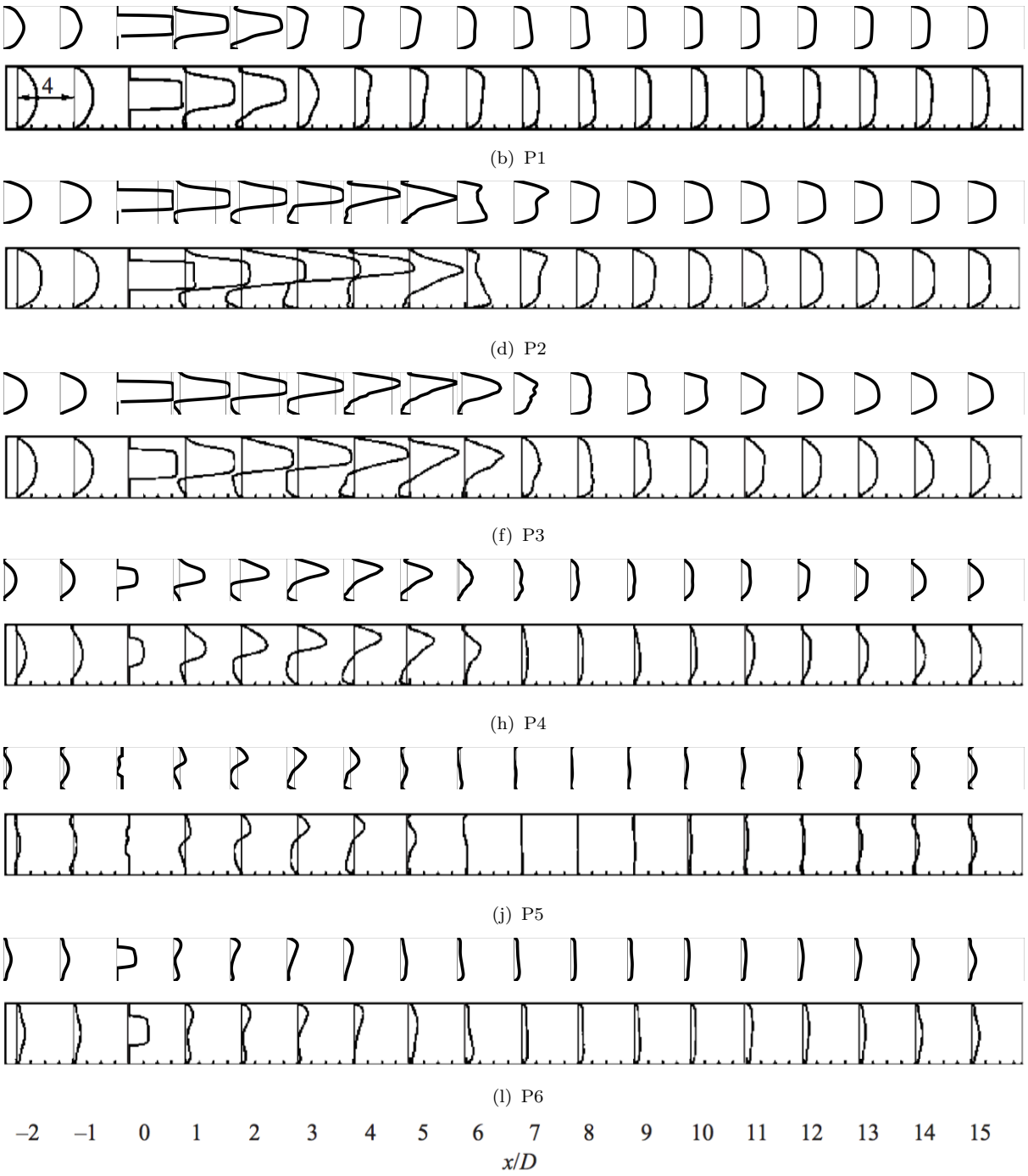

Figure 5: Sequence of ensemble-averaged axial velocity profiles, $\langle u \rangle / u_c$ at observation points P1-P6 (top down) in the x-z plane. The top row of each point depicts computations from *Musubi* followed by the corresponding image from the benchmark computations from NEK5000.

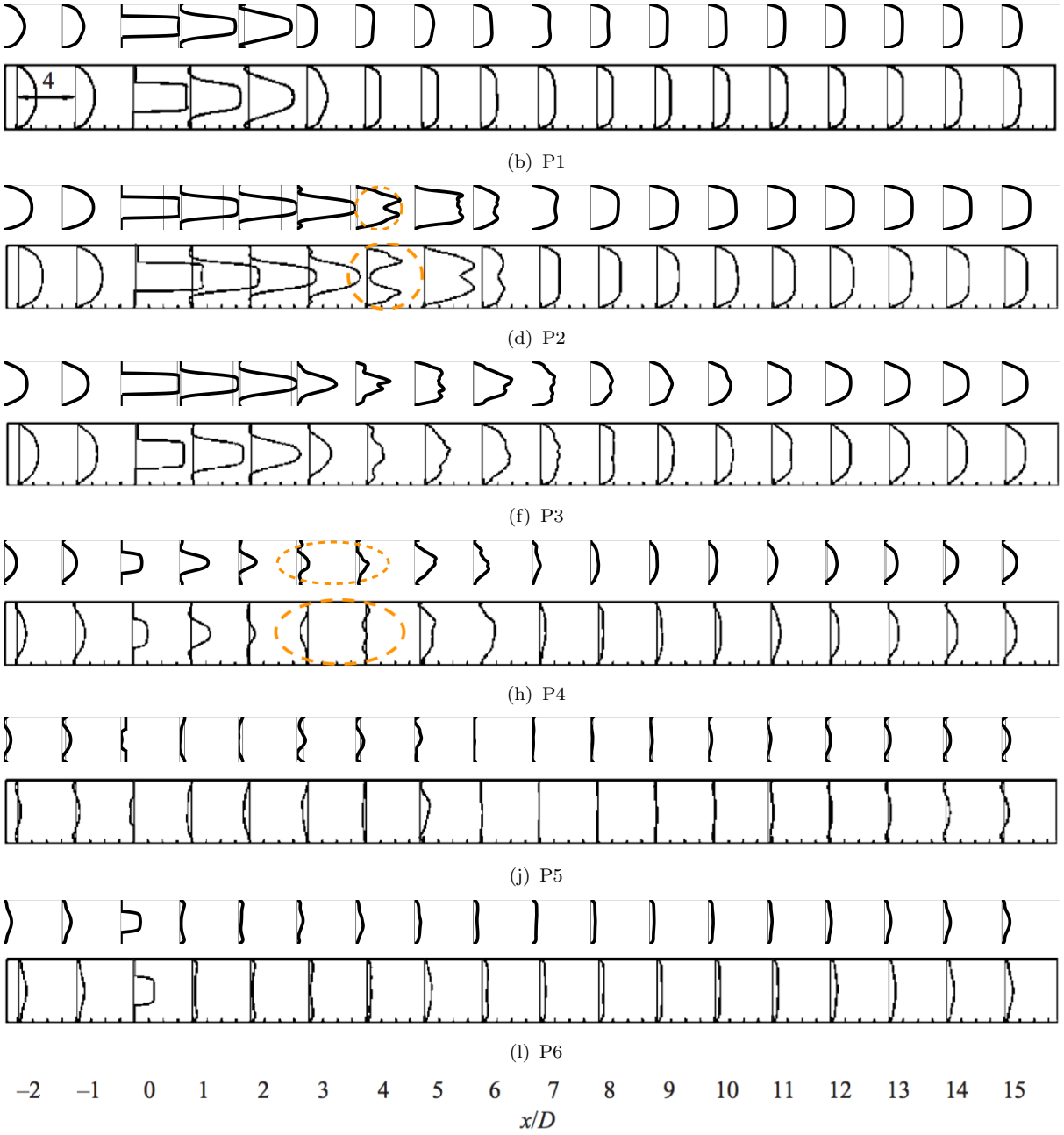

Figure 6: Sequence of ensemble-averaged axial velocity profiles, $\langle u \rangle / u_c$ at observation points P1-P6 (top down) in the x-y plane. The top row of each point depicts computations from *Musubi* followed by the corresponding image from the benchmark computations from NEK5000.

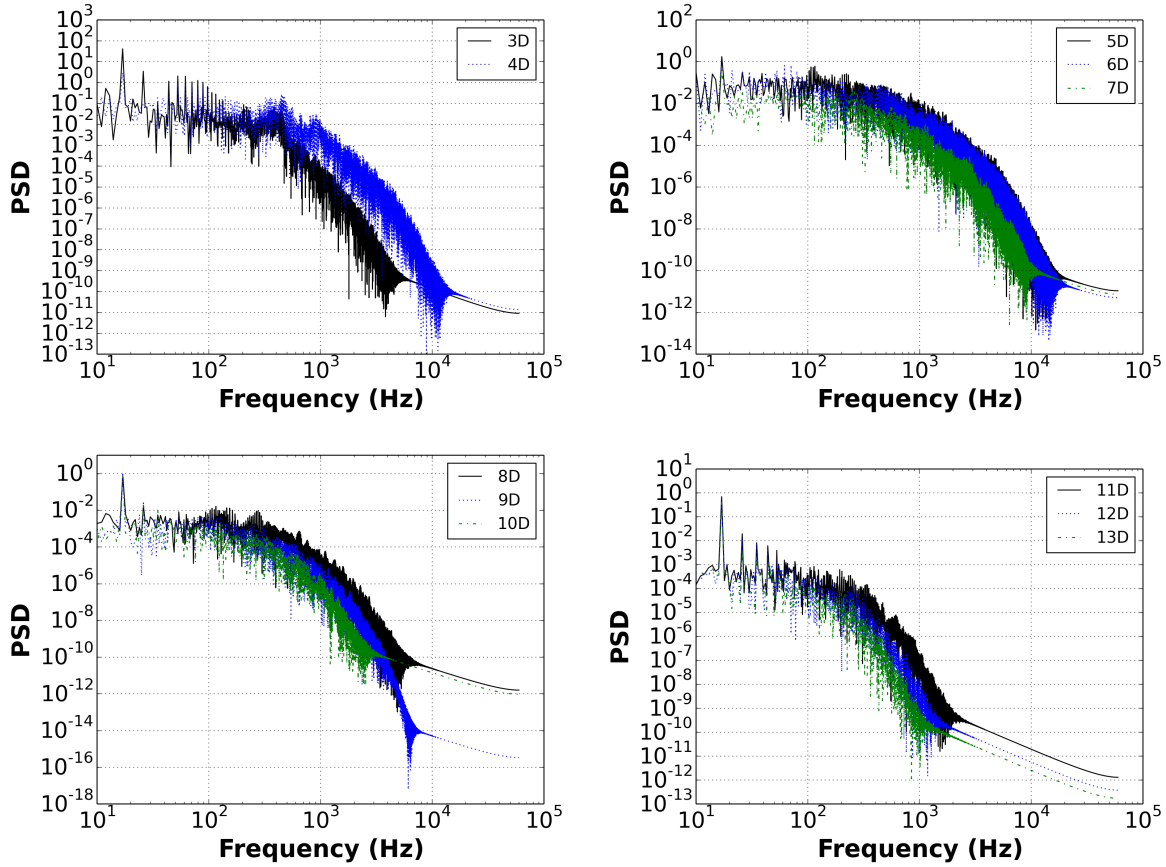

Figure 7: Energy spectra of the turbulent kinetic energy computed at the centerline from LR simulations. The locations represent distance in diameters from the stenosis.

Turbulent Characteristics of the Flow

Figure 7 shows the frequency spectra of the turbulent kinetic energy computed from centerline axial velocity at varying distance from the stenosis throat from LR simulations whereas figure 8 shows the same from HR simulations. The fluctuations are higher at locations x=3-6D and the flow starts to re-laminarize beyond x=9D – an observation that is consistent with the instantaneous and ensemble averaged velocity fields. The spectra at these locations indicate a large number of frequencies in the inertial subrange. The viscosity starts to dominate at frequencies of $\sim 10^4$ Hz. At locations $x > 10D$, flow can be considered largely laminar as the PSD is mostly below 10^{-10} for frequencies more than 10^3 Hz.

Comparison of the power spectrum plots from LR and HR simulations reveals a generic pattern whereby higher frequencies are detected by HR simulations due to small δt. The qualitative patterns are similar for both resolutions and as discussed later, the choice of resolutions is generally case dependent.

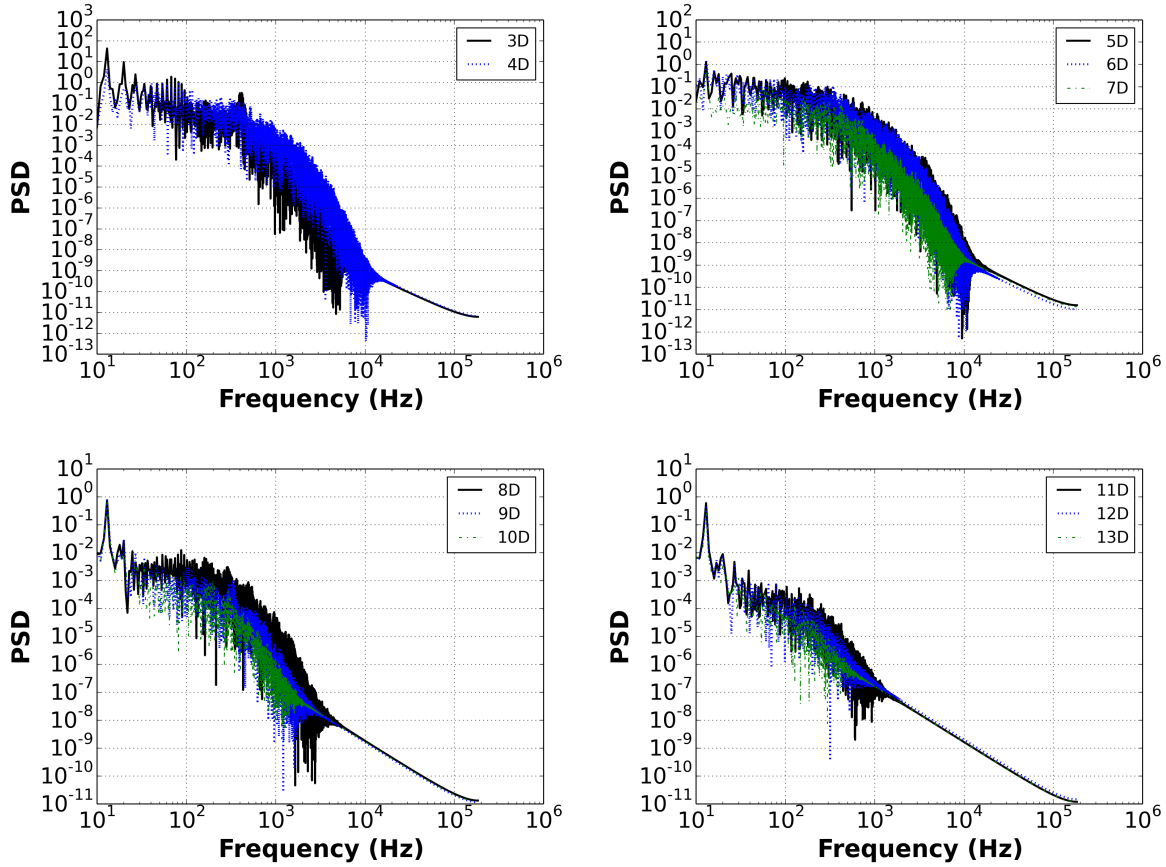

Figure 8: Energy spectra of the turbulent kinetic energy computed at the centerline from HR simulations. The locations represent distance in diameters from the stenosis.

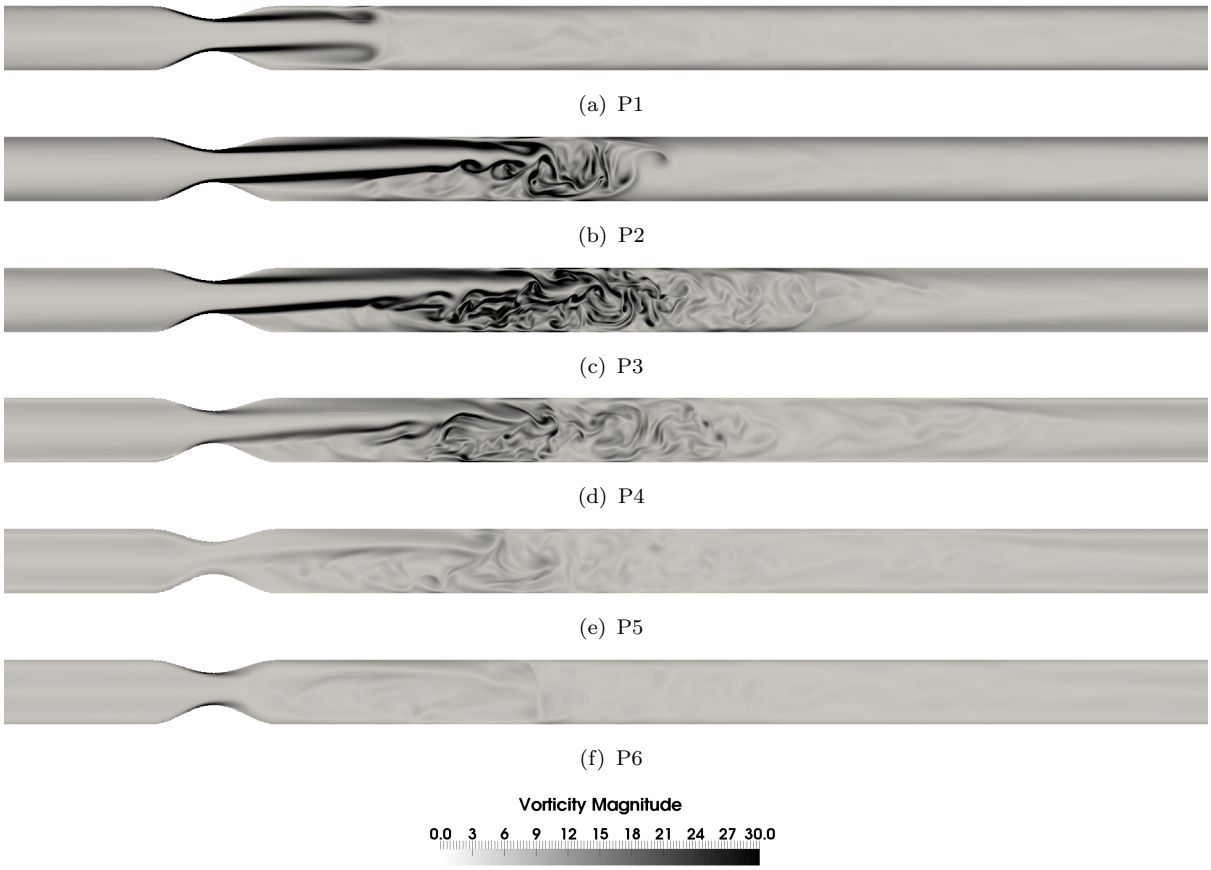

Figure 9: Ensemble averaged vorticity magnitude, normalized by u_c/D at the x-z plane. Ensemble averaging is performed for ONLY $n = 3$ cycles to observe the intricate vortices which smear out when larger number of cycles are taken into account.

Vortex structures

Figure 9 and 10 show the ensemble averaged vorticity magnitude across the xz and xy planes respectively from LR simulations [5]. The main patterns look similar to Varghese *et al.*[28], though LBM has detected some miniature vortices due to higher spatial and temporal magnitudes. When ensemble average for larger number of cycles is taken, the vortices are expected to die away and mimic Varghese *et al.*[28] a bit more closely.

Figure 11 shows the vortex structures at 4 observation points during the 20th cycle for LR simulations. The vortices are educed by the Q-criterion discussed in subsection 2. The vortices begin to die during P5 and P6 due to re-laminarization of flow and are thus not shown in this figure. It is also interesting to observe that the location of vortices is along $x > 4D$ where the flow transits to main-stream turbulence, and was also reminiscent

[5]It should be explicitly mentioned that the ensemble average for $n = 3$ cycles only is taken to educe the vortices, which would otherwise be smeared out for larger number of cycles

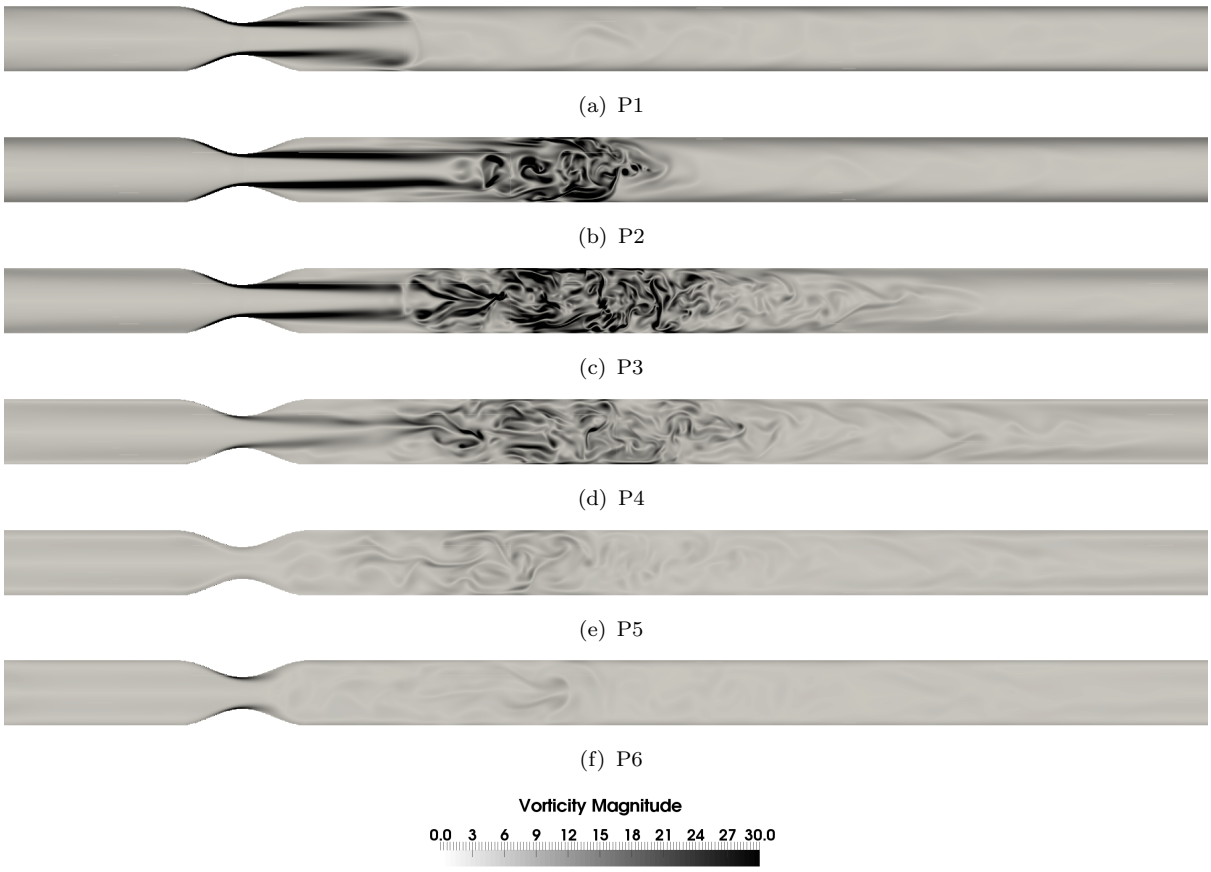

(a) P1

(b) P2

(c) P3

(d) P4

(e) P5

(f) P6

Figure 10: Ensemble averaged vorticity magnitude, normalized by u_c/D at the x-y plane. Ensemble averaging is performed for ONLY $n = 3$ cycles to observe the intricate vortices which smear out when larger number of cycles are taken into account.

(a) P1

(b) P2

(c) P3

(d) P4

Figure 11: Velocity colored Q-isosurfaces (Q=0.4) at the observation points P1-P4 during the 20th cycle for LR resolution. The velocity is normalized by u_c.

	δx	δt	l^+	t^+
LR	64	30×10^{-6}	2.67	0.84
HR	32	7.5×10^{-6}	1.10	0.53

Table 2: The ratio of spatio-temporal scales (l^+, t^+) in the simulation and the Kolmogorov microscales for different resolutions.

in the PSD plots.

Kolmogorov microscales

Table 2 lists the l^+ and t^+ for LR and HR simulations. The ration are computed at the observation point P2 along x=4D during the 20th cycle as the fluctuation in strain rate was maximal at this location during P2, which implies maximum dissipation during the whole simulation. The employed resolutions are ample to resolve the rapidly varying structures expected in a turbulent flow[18]. Whereas the δx of LR is $\sim$ 3 times of the Kolmogorov length scale, in a minor transitional flow in relatively less complex geometry like the presented stenosis, it should be enough for simulations.

4 Discussion

Analysis of the flow

Main things to observe (and compare to[28]) from the flow patterns of figure 5 and 6 were flow direction, peaks and nadirs as well as zones of flow reversal or recirculation. The flow field in the x-z plane seemed to agree well with.[282007Varghese *et al.*Varghese, Frankel & Fischer The velocity was elevated at the throat of the stenosis, remained high in post-stenotic regions before becoming nearly constant near the end regions of the channel ($x > 11D$).

Similar agreement was seen for the x-y plane – though there were a few locations of disparity. For example, the post stenotic field at P2 (x=4) looked very different from Varghese *et al.*[28] (highlighted in orange circles). At P4, even the direction of flow disagreed at x=3 and x=4, which is very surprising especially after an excellent agreement seen for x-z plane. The exact reason for this mismatch cannot be stated but it can be attributed to the different solution algorithms where minor differences are obvious. It should also be kept in mind that this comparison is one of *statistics* and involves round-off errors. Moreover, the perturbation that might be introduced as a result of wall roughness may stay in the flow up to an arbitrary number of cycles before being washed out completely. The boundary layer resolved by LBM and Spectral methods can be very different due to the different algorithms, and accuracy of one over the other can not be distinctly stated. The regions that are up-stream of stenosis and in its vicinity have very high velocity gradients due to the onset of transition, and the wall boundary conditions are expected to influence the results dramatically. Whats most contenting is that in spite

of different flow directions in these two locations, the flow field re-attained similarity beyond x=5 at all the time points, as did the flow field right at the stenosis throat.

Also, the flow fields from *Musubi* looked exactly the same as those from NEK5000 at P6 which portrays that the discrepancies seen during P4 and P5 might have been a result of the loss of coherence patterns caused by large decelerative forces, which were then overcame by the stabilization resulted by acceleration of flow. It is expected that if ensemble averaging over a larger number of cycles is done, these effects would wash away and the disparities would eventually vanish. That however is not considered important due to the convincing agreement in other locations and time points, and would make sense when the simulation is actually re-conducted with NEK5000 as well.

Particularly interesting was the similarity in the patterns during P2 where the velocity of inflow is maximum, and P6 where the flow is in mid-acceleration phase after the deceleration. The presence of higher vortices during P3 than P2 as educed by the Q-Criterion (figure 11) appeared surprising at a first glance. From figure 2 one would expect highest vortices during P2 since it is the point with peak velocity. This is a consequence of the large decelerative forces that results in chaotic flow between P2 and P3 and creates distinct and larger vortex envelopes during P3. This was also observed in vorticity plots of figure 9 and figure 10.

The vorticity plots in figure 9 and 10 show some minute vortices in post stenotic areas even after ensemble averaging (though for only $n = 3$ cycles). The overall vorticity patterns are exactly similar to Varghese *et al.*[28] and the subtle differences are attributed to resolutions and visualization techniques as information about visualization software/method used by[28] is not known.

Role of employed resolutions

As was seen from figures 3(a) and 3(b), the employment of high resolutions, that was directly at the order of Kolmogorov length and time scales (table 2), did not provide much *improvement* to the simulated flow field except for capture of some rapid spatial and temporal scales. The consumption of memory and compute time on the other hand became ~ 8 times with a higher resolution. An unequivocal remark whether LR indeed is enough for simulating transitional flows in general, and transitional physiological flows in particular can not be made because physiological geometries are generally extremely complex. It has been shown in our studies of transitional aneurysmal flows that the solution indeed does change upon refinements when the geometry is not a regular conduit but a complex geometry[11;10]. Choice of resolutions in fact has been a subject of discussion with other numerical techniques as well, see for example research on this aspect about blood flow in aneurysms[26;29;25] as well as simulation of the cerebrospinal fluid in spinal canals[8].

In addition to that, the stenosis geometry studied here has one outflow which is perpendicular to the incoming flow. Presence of more outlets as well as the angle at which

flow attacks these outlets is likely to upsurge the resolution requirements. Moreover, the stenosis may be viewed as a *controlled distortion* in a straight cylindrical pipe which is located at only one location in the pipe. Presence of such distortions at multiple locations as well as their irregularity can educe phenomena like flow separation and hydraulic jumps which would require employment of higher resolutions.

This study would be unable to establish the superiority of one numerical method over other as such a pursuit would require execution of different numerical codes on the same machine, and would require that the computer science methodologies followed in implementation of the said codes are in agreement. One thing that enforces superiority of spectral methods is its ability to increase effective resolution[24] by increasing the polynomial order. Also Varghese *et al.*[28] employed higher mesh density near the walls and the stenosis throat unlike the even mesh employed by me in this study. Local grid refinement[7;6] is implemented and validated in *Musubi* framework and an accurate gauge on resolution/memory requirements can be accomplished only by exploring those techniques. What seems obvious at this point is that very low resolutions would suffice for an accurate simulation of hydrodynamics in the post stenotic regions beyond $x > 10D$, where the flow relaminarized and did not exhibit much spatial and temporal variations.

A mentionable aspect of this study in particular, and LBM simulated flows in general is the initial transients. I had to discard the initial 2 cycles from the analysis as they contain some spurious oscillations before converging to a physically meaningful outcome. For these limitations of LBM, it has generally been considered unsuitable for steady problems and its inherently transient nature makes it a suited method for time dependent flows[21;4]. I shall not delve into details of the initial transients analysis of other methods, and a brief account for that can be found in[21;4].

Outlook

The present work re-validates LBM and *Musubi* particularly for transitional flows. The study has scope for improvement in the following areas:

1. Computational comparison of NEK5000 and *Musubi*
2. Comparison of LBM with other methods like FVM and FEM
3. Investigation of local grid refinement in *Musubi*
4. Extension of this study for bi-directional pulsating flows
5. Extension of the study for high Re fully developed turbulent flows

A final remark that can be made is that a LBM simulation on the same geometry with 8×10^6 cells was conducted using *Musubi* on my personal laptop, which completed one cycle in $\sim$ 26 hours. The fluctuations captured were less intense than the presented DNS,

albeit the qualitatively agreement was very good. This suggests that with improving computer architectures, one might be able to simulate such problems on local computers with appreciable ease in future.

Acknowledgements

Thanks to *Prof. Kent-André Mardal* and *Prof. Sabine Roller* for supervision in my doctoral studies.

The study was suggested and motivated by *Dr. Bryn Martin* and *Mr. Soroush Heidari Pahlavian*. Soroush also helped me in creating the geometry and understanding the original benchmark.

I am specially thankful to the High Performance Computing Center, Stuttgart, Germany for compute resources on *Hazel Hen* and to the Leibniz Supercomputing Center, Munich, Germany for compute resources on the *SuperMUC*.

References

[1] Ahmed, Saad A & Giddens, Don P 1983 Velocity measurements in steady flow through axisymmetric stenoses at moderate reynolds numbers. *Journal of biomechanics* **16** (7), 505–516.

[2] Ahmed, Saad A & Giddens, Don P 1984 Pulsatile poststenotic flow studies with laser doppler anemometry. *Journal of biomechanics* **17** (9), 695–705.

[3] Durbin, Paul A & Reif, BA Pettersson 2011 *Statistical theory and modeling for turbulent flows*. John Wiley & Sons.

[4] Geller, Sebastian, Krafczyk, Manfred, Tölke, Jonas, Turek, Stefan & Hron, Jaroslav 2006 Benchmark computations based on lattice-boltzmann, finite element and finite volume methods for laminar flows. *Computers & Fluids* **35** (8), 888–897.

[5] Harlacher, Daniel F., Hasert, Manuel, Klimach, Harald, Zimny, Simon & Roller, Sabine 2012 Tree based voxelization of stl Data. In *High Performance Computing on Vector Systems 2011*, pp. 81–92.

[6] Hasert, Manuel 2014 Multi-scale lattice boltzmann simulations on distributed octrees. PhD thesis, Aachen, Techn. Hochsch., Diss., 2013.

[7] Hasert, Manuel, Masilamani, Kannan, Zimny, Simon, Klimach, Harald, Qi, Jiaxing, Bernsdorf, Jörg & Roller, Sabine 2013 Complex fluid simulations with the parallel tree-based lattice boltzmann solver musubi. *Journal of Computational Science* .

[8] Helgeland, Anders, Mardal, Kent-Andre, Haughton, Victor & Anders Pettersson Reif, Bjørn 2014 Numerical simulations of the pulsating flow of cerebrospinal fluid flow in the cervical spinal canal of a chiari patient. *Journal of Biomechanics* .

[9] Hunt, Julian CR, Wray, AA & Moin, Parviz 1988 Eddies, streams, and convergence zones in turbulent flows. In *Studying Turbulence Using Numerical Simulation Databases, 2*, , vol. 1, pp. 193–208.

[10] Jain, Kartik & Mardal, Kent-Andre 2015 Exploring the critical reynolds number for transition in intracranial aneurysms - highly resolved simulations below kolmogorov scales (0), 560 – 563, 2015 Computational and Mathematical Biomedical Engineering.

[11] Jain, Kartik, Roller, Sabine & Mardal, Kent-André 2015 Transitional flow in intracranial aneurysms – a space and time refinement study below the kolmogorov scales using lattice boltzmann method. *Computers & Fluids (In Revision)* .

[12] Junk, Michael, Klar, Axel & Luo, Li-Shi 2005 Asymptotic analysis of the lattice boltzmann equation. *Journal of Computational Physics* **210** (2), 676–704.

[13] Junk, Michael & Yang, Zhaoxia 2011 Asymptotic Analysis of Lattice Boltzmann Outflow Treatments. *Communications in Computational Physics* pp. 1–11.

[14] Klimach, Harald, Jain, Kartik & Roller, Sabine 2014 End-to-end parallel simulations with apes. In *Parallel Computing: Accelerating Computational Science and Engineering (CSE)*, , vol. 25, pp. 703–711.

[15] Lallemand, Pierre & Luo, Li-Shi 2000 Theory of the lattice boltzmann method: Dispersion, dissipation, isotropy,galilean invariance, and stability. *Physical Review E* **61** (6), 6546.

[16] Lallemand, Pierre & Luo, Li-Shi 2003 Theory of the lattice boltzmann method: Acoustic and thermal properties in two and three dimensions. *Physical review E* **68** (3), 036706.

[17] Latt, Jonas 2007 Hydrodynamic limit of lattice boltzmann equations. PhD thesis, University of Geneva.

[18] Moin, Parviz & Mahesh, Krishnan 1998 Direct numerical simulation: a tool in turbulence research. *Annual review of fluid mechanics* **30** (1), 539–578.

[19] Nash, Rupert W, Carver, Hywel B, Bernabeu, Miguel O, Hetherington, James, Groen, Derek, Krüger, Timm & Coveney, Peter V 2014 Choice of boundary condition for lattice-boltzmann simulation of moderate-reynolds-number flow in complex domains. *Physical Review E* **89** (2), 023303.

[20] Pope, Stephen B 2000 *Turbulent flows*. Cambridge university press.

[21] Rheinländer, Martin 2007 Analysis of lattice-boltzmann methods .

[22] Robinson, Stephen Kern 1991 The kinematics of turbulent boundary layer structure. *NASA STI/Recon Technical Report N* **91**, 26465.

[23] Roller, Sabine, Bernsdorf, Jörg, Klimach, Harald, Hasert, Manuel, Harlacher, Daniel, Cakircali, Metin, Zimny, Simon, Masilamani, Kannan, Didinger, Laura & Zudrop, Jens 2012 An adaptable simulation framework based on a linearized octree. In *High Performance Computing on Vector Systems 2011*, pp. 93–105.

[24] Succi, Sauro, Benzi, Roberto & Higuera, Francisco 1991 The lattice boltzmann equation: a new tool for computational fluid-dynamics. *Physica D: Nonlinear Phenomena* **47** (1), 219–230.

[25] Valen-Sendstad, Kristian, Mardal, Kent-Andre, Mortensen, Mikael, Reif, Bjørn Anders Pettersson & Langtangen, Hans Petter 2011 Direct numerical simulation of transitional flow in a patient–specific intracranial aneurysm. *Journal of Biomechanics* **44** (16), 2826–2832.

[26] Valen-Sendstad, K & Steinman, DA 2013 Mind the gap: Impact of computational fluid dynamics solution strategy on prediction of intracranial aneurysm hemodynamics and rupture status indicators. *American Journal of Neuroradiology* .

[27] Varghese, Sonu S, Frankel, Steven H & Fischer, Paul F 2007 Direct numerical simulation of stenotic flows. part 1. steady flow. *Journal of Fluid Mechanics* **582**, 253–280.

[28] Varghese, Sonu S, Frankel, Steven H & Fischer, Paul F 2007 Direct numerical simulation of stenotic flows. part 2. pulsatile flow. *Journal of Fluid Mechanics* **582**, 281–318.

[29] Ventikos, Y 2014 Resolving the issue of resolution. *American Journal of Neuroradiology* **35** (3), 544–545.